Star Cluster Formation and Evolution in Nearby Starburst Galaxies: I. Systematic Uncertainties

R. de Grijs[1]⋆, U. Fritze–v. Alvensleben[2], P. Anders[2], J.S. Gallagher III[3],
N. Bastian[4], V.A. Taylor[5], R.A. Windhorst[5]

[1] *Institute of Astronomy, University of Cambridge, Madingley Road, Cambridge CB3 0HA*
[2] *Universitätssternwarte, University of Göttingen, Geismarlandstr. 11, 37083 Göttingen, Germany*
[3] *Astronomy Department, University of Wisconsin-Madison, 475 N. Charter St., Madison, WI 53706, USA*
[4] *Astronomical Institute, Utrecht University, Princetonplein 5, 3584 CC Utrecht, The Netherlands*
[5] *Department of Physics & Astronomy, Arizona State University, Box 871504, Tempe, AZ 85287-1504, USA*

arXiv:astro-ph/0302286v1 14 Feb 2003

ABSTRACT

The large majority of extragalactic star cluster studies done to date have essentially used two or three-passband aperture photometry, combined with theoretical stellar population synthesis models, to obtain age, mass and extinction estimates, and sometimes also metallicities. The accuracy to which this can be done depends on the choice of (broad-band) passband combination and, crucially, also on the actual wavelengths and the wavelength range covered by the observations. Understanding the inherent systematic uncertainties (the main aim of this paper) is of the utmost importance for a well-balanced interpretation of the properties of extragalactic star cluster systems. We simultaneously obtain ages, metallicities and extinction values for ~ 300 clusters in the nearby starburst galaxy NGC 3310, based on archival *Hubble Space Telescope* observations from the ultraviolet (UV) to the near-infrared (NIR). We show that, for ages $6 \lesssim \log(\text{age/yr}) \lesssim 9$, and if one can only obtain partial coverage of the spectral energy distribution (SED), an optical passband combination of at least four filters including *both* blue *and* red passbands results in the most representative age distribution, as compared to the better constrained ages obtained from the full UV–NIR SED coverage. We find that while blue-selected passband combinations lead to age distributions that are slightly biased towards younger ages due to the well-known age–metallicity degeneracy, red-dominated passband combinations should be avoided. NGC 3310 underwent a (possibly extended) global burst of cluster formation $\sim 3 \times 10^7$ yr ago. This coincides closely with the last tidal interaction or merger with a low-metallicity galaxy that likely induced the formation of the large fraction of clusters with (significantly) subsolar metallicities. The logarithmic slope of the *V*-band cluster luminosity function, for clusters in the range $17.7 \lesssim \text{F606W} \lesssim 20.2$ mag, is $\alpha_{\text{F606W}} \simeq -1.8 \pm 0.4$. The observed cluster system has a median mass of $\langle \log(m/M_\odot) \rangle \simeq 5.25 \pm 0.1$, obtained from scaling the appropriate model SEDs for known masses to the observed cluster SEDs.

Key words: HII regions – galaxies: evolution – galaxies: individual: NGC 3310 – galaxies: interactions – galaxies: starburst – galaxies: star clusters

1 THE CLUSTER LUMINOSITY FUNCTION

1.1 Introduction

Cluster luminosity functions (CLFs) and colour distributions are the most important diagnostics in the study of globular and compact star cluster populations in nearby galaxies. For the old globular cluster (GC) systems in, e.g., the Galaxy, M31, M87, and old elliptical galaxies, the CLF shape is well-established: it is roughly Gaussian, with the peak or turnover magnitude at $M_V^0 \simeq -7.4$ mag and a Gaussian FWHM of ~ 3 mag (Whitmore et al. 1995, Harris 1996, 2001, Ashman & Zepf 1998, Harris, Harris & McLaughlin 1998). The well-studied young star cluster (YSC) population in the LMC and the Galactic open cluster system, on

⋆ E-mail: grijs@ast.cam.ac.uk

the other hand, display a power-law CLF (Elson & Fall 1985, Harris & Pudritz 1994, Elmegreen & Efremov 1997).

Hubble Space Telescope (HST) observations are continuing to provide an ever increasing number of CLFs for compact YSC systems in galaxies beyond the Local Group and the Virgo cluster (e.g., Whitmore & Schweizer 1995, Schweizer et al. 1996, Miller et al. 1997, Zepf et al. 1999, de Grijs, O'Connell & Gallagher 2001, Whitmore et al. 2002). Although a large number of studies have attempted to detect a turn-over in young or intermediate-age CLFs, the shapes of such young and intermediate-age CLFs have thus far been consistent with power laws down to the observational completeness thresholds (but see Miller et al. 1997, de Grijs et al. 2001, 2003a,b).

1.2 Evolutionary Effects?

The striking difference between the power-law distributions for young star clusters and the Gaussian distribution of the old Galactic GCs has recently attracted renewed theoretical attention. The currently most popular (but, admittedly, speculative) GC formation models suggest that the distribution of the initial cluster masses is closely approximated by a power law (e.g., Harris & Pudritz 1994, McLaughlin & Pudritz 1996, Elmegreen & Efremov 1997, Gnedin & Ostriker 1997, Fall & Zhang 2001).

Which processes will affect the CLFs such that they transform from a power-law shape to a Gaussian distribution? It is generally assumed that the processes responsible for the depletion of a star cluster population over time-scales of a Hubble time include the preferential depletion of low-mass clusters both by evaporation due to two-body relaxation and by tidal interactions with the gravitational field of their host galaxy (e.g., Fall & Rees 1977, 1985, Elmegreen & Efremov 1997, Murali & Weinberg 1997a,b,c, Ostriker & Gnedin 1997, Harris et al. 1998, Fall & Zhang 2001), and the preferential disruption of high-mass clusters by dynamical friction (Vesperini 2000, 2001). From the currently most popular GC evolution models it follows that *any* initial mass (or luminosity) distribution will shortly be transformed into a peaked distribution, although it should be noted that these models apply only to Milky Way-type conditions in which the GC system is characterised by significant radially dependent radial anisotropy. Vesperini (2000, 2001) has included the internal gravitational interactions between cluster stars in his models and concludes that these need considerable fine tuning to transform a power law initial cluster mass function (ICMF) into a Gaussian distribution, whereas a Gaussian ICMF conserves its shape rather independently of the choice of parameters: destruction of low-mass clusters by evaporation and the tidal field is balanced by the destruction of high-mass clusters through dynamical friction.

1.3 Interacting galaxies

All of these models are valid *only* for Milky Way-type gravitational potentials, however. Galaxy-galaxy interactions will obviously have a major effect on the resulting gravitational potential, in which the dynamical star cluster evolution is likely significantly different (see, e.g., Boutloukos & Lamers 2003, de Grijs et al. 2003a).

The mass spectrum of molecular clouds or molecular cloud cores, progenitors of young star clusters, has never been determined in interacting galaxies to similarly faint limits as in the Milky Way and the Magellanic Clouds. The significant external pressure in interacting gas-rich galaxies may be expected to have a major effect on the molecular cloud mass spectrum.

Significant age spread effects in young cluster systems – in which cluster formation is still ongoing – affect the observed CLF (Meurer 1995, Fritze–v. Alvensleben 1998, 1999, de Grijs et al. 2001, 2003a,b), which might in fact make an intrinsically Gaussian CLF (or ICMF) appear as a power-law CLF (see, e.g., Miller et al. 1997, Fritze–v. Alvensleben 1998). It is obviously very important to age date the individual clusters and to correct the observed CLF to a common age, before interpreting the CLF (Fritze–v. Alvensleben 1999, de Grijs et al. 2001, 2003a,b), in particular if the age spread within a cluster system is a significant fraction of the system's mean age.

In de Grijs et al. (2003a,b), we provide the first observational evidence for a clear turn-over in the intermediate-age CLF of the clusters formed *in the burst of cluster formation* in M82's fossil starburst region "B", which very closely matches the universal CLFs of old GC systems. This provides an important test of cluster disruption models (see de Grijs et al. 2003b).

1.4 Star cluster metallicities

Metallicities of YSCs produced in galaxy interactions, mergers or starbursts are an important discriminator against GCs formed in the early Universe. They are expected to correspond to the interstellar medium (ISM) abundances of the interacting/starburst galaxies, and are therefore most likely significantly higher than those of halo GCs in the Milky Way and other galaxies with old GC systems. ISM abundances span a considerable range, however, among different galaxy types from Sa through Sd, irregular, and dwarf galaxies, and may exhibit significant radial gradients (Oey & Kennicutt 1993, Zaritsky, Kennicutt & Huchra 1994, Richer & McCall 1995). Many of these galaxies show abundance gradients, which have recently been shown to sometimes extend considerably beyond their optical radii (Ferguson et al. 1998, van Zee et al. 1998). However, from those large radii, gas can be funneled efficiently into the inner regions during galaxy interactions and mergers (e.g., Hibbard & Mihos 1995).

Hence, a considerable metallicity range may be expected for YSCs produced in interactions of various types of galaxies and even among the YSCs formed within one global galaxy-wide starburst.

During a strong burst, typically lasting a few $\times 10^8$ yr in a massive gas-rich galaxy, a significant increase of the ISM abundance may occur (Fritze–v. Alvensleben & Gerhardt 1994, their Fig. 12b). Meanwhile, some fraction of the gas enriched by dying first-generation burst stars may well be shock-compressed to cool fast enough to be built into later generations of stars or clusters produced in the burst. The same effect may occur when multiple bursts occur in a series of close encounters between two galaxies before their final merger. Hence, in extended starburst episodes metallicity differences between YSCs formed early on and late in the burst phase may be expected.

Precise (relative) metallicity determinations for individual YSCs are not only important to study the questions raised above, but also for the correct derivation of ages from broad-band colours.

Dust extinction is often very important in YSC systems. In particular the youngest post-burst galaxies and galaxies with ongoing starbursts often show strong and patchy dust structures and morphologies. For instance, the youngest clusters in the overlap region of the two galactic discs in the Antennae galaxies are completely obscured in the optical and can only be detected in near or mid-infrared observations (Mirabel et al. 1998, Mengel et al. 2001). Older merger remnants like NGC 7252 or NGC 3921 seem to have blown their inner regions clear of all the gas left over from intense star formation during the burst (e.g., Schweizer et al. 1996). Extinction estimates towards individual YSCs are therefore as important as individual metallicity estimates in order to obtain reliable ages and to be able to derive an age-normalised CLF or YSC mass function.

1.5 Spectroscopy vs. multi-passband photometry

Individual YSC spectroscopy, feasible today with 8m-class telescopes for the nearest systems, is very time-consuming, since observations of large numbers of clusters are required to obtain statistically significant results. Multi-passband imaging is a very interesting and useful alternative, as we will show below, in particular if it includes coverage of near-infrared (NIR) and/or ultraviolet (UV) wavelengths. The large majority of extragalactic star cluster studies done to date have essentially used two or three-passband aperture photometry, combined with theoretical stellar population synthesis models to obtain age estimates. The accuracy to which this can be done obviously depends on the number of different (broad-band) filters available as well as, crucially, on the actual wavelengths and wavelength range covered by the observations, and on the PSF size compared to the cluster surface density profile (i.e., on how close to the observations were taken to the confusion limit for these clusters).

In this paper we assess the systematic uncertainties in age, extinction and metallicity determinations for YSC systems inherent to the use of broad-band, integrated colours. We have developed an evolutionary synthesis optimisation technique that can be applied to photometric measurements in a given number $N(N \geq 4)$ of broad-band passbands. The optimisation routine then simultaneously determines the best combination of age, extinction and metallicity from a comparison with the most up-to-date Göttingen simple stellar population (SSP) models (Schulz et al. 2002), to which we have added the contributions of an exhaustive set of gaseous emission lines and gaseous continuum emission (Anders, Fritze–v. Alvensleben & de Grijs 2002, Anders & Fritze–v. Alvensleben 2003). We also compare these results with similar determinations based on the Starburst99 SSP models (Leitherer et al. 1999), but assuming fixed, solar metallicity for our sample clusters. Although this is an often-used assumption, we will show that this introduces significant systematic effects in the final age distribution, and therefore also in the mass distribution.

We decided to focus our efforts on the nearby, well-studied starburst galaxy NGC 3310, known to harbour large numbers of young star clusters, for which multi-passband ob-

Table 1. Overview of the *HST* observations of NGC 3310

Filter	Exposure time (sec)	Centre[a]	PID[b]	ORIENT[c] (°)
F300W	900,1000	WF3	8645	−150.282
F336W	2×500	PC	6639	−144.232
F439W	2×300	PC	6639	−144.232
F606W	500	PC	5479	145.553
F814W	160,180	PC	6639	−144.232
	100,160	WF3	8645	−150.282
F110W	2×159.96	NIC2	7268	80.519
F160W	2×191.96	NIC2	7268	80.519

NOTES: [a] – Location of the galactic centre; [b] – *HST* programme identifier; [c] – Orientation of the images (taken from the image header), measured North through East with respect to the V3 axis (i.e., the X=Y diagonal of the WF3 CCD +180°).

servations from the near-UV to the NIR are readily available from the *HST* Data Archive (Section 2; see also Elmegreen et al. 2002, hereafter E02). In Section 4 we first place the NGC 3310 starburst in its physical context. We then discuss the derived age distribution of the cluster population, which we extend compared to previous work, in terms of the evolution of the CLF and the interaction stage of its parent galaxy in Sections 5 and 6. We summarise our main results and conclusions in Section 7. Finally, we will apply our knowledge of the systematic uncertainties gained in this paper to a larger sample of nearby starburst and interacting galaxies drawn from the *HST* GO-8645 programme (Windhorst et al. 2002) in Papers II and III (de Grijs et al., in prep.).

2 OBSERVATIONS AND DATA PREPARATION

NGC 3310 is a representative member of the class of galaxies often showing signs of active starbursts and recently formed star clusters. The galaxy may have been a normal, quiescent Sbc-type galaxy before it started to produce large numbers of new stars, possibly due to the merger with a gas-rich low-metallicity companion (cf. Kobulnicky & Skillman 1995).

As part of *HST* programme GO-8645, we obtained observations of NGC 3310 through the F300W ("UV") and F814W filters (Windhorst et al. 2002), with the galaxy centre located on chip 3 of the Wide Field Planetary Camera 2 (*WFPC2*). Observations in additional passbands were obtained from the *HST* Data Archive. In order to obtain the largest common field of view (FoV) in the optical wavelength range, we restricted these archival data to be taken with the *WFPC2*. In addition, we obtained archival NIR images taken with the Near-Infrared Camera and Multi-Object Spectrometer's (NICMOS) camera 2, which provides the best compromise of spatial resolution ($0\overset{''}{.}075$ pixel^{-1}) and FoV ($19\overset{''}{.}2 \times 19\overset{''}{.}2$) when combined with *WFPC2* observations (see below). We have summarized the combined set of *HST* observations through broad-band filters used in this paper in Table 1.

Pipeline image reduction and calibration of the *WFPC2* images were done with standard procedures provided as part of the IRAF/STSDAS[†] package, using the updated and cor-

[†] The Image Reduction and Analysis Facility (IRAF) is dis-

rected on-orbit flat fields and related reference files most appropriate for the observations.

We first registered the individual images obtained for a given programme and created combined images for each programme/passband combination, using the appropriate IMALIGN and IMCOMBINE routines in IRAF. Next, we rotated all of these combined images to a single orientation using objects in common among the observed fields, applying IRAF's ROTATE and IMGEOM routines. We used the observations of programme GO-6639 as basis for these rotations. Finally, we adjusted the pixel size of both the PC and the NICMOS/2 images to that of the final, rotated WF3 images. The final pixel size for all images is $0\rlap{.}''0998$.

Because of the significantly smaller FoV of the NICMOS observations, we created two sets of final, registered images: one set containing the *WFPC2* images only, and a second set consisting of all aligned images (*WFPC2* and NICMOS). The resulting combined "*WFPC2*-only" FoV is 331×323 pixels ($33\rlap{.}''03 \times 32\rlap{.}''24$). Similarly, the common FoV for all instrument/passband combinations is 226×227 pixels ($22\rlap{.}''55 \times 22\rlap{.}''65$).

2.1 Source selection

We based our initial selection of sources on a customized version of the DAOFIND task in the DAOPHOT software package (Stetson 1987), as running under IDL.

We obtained initial source lists for all available passbands, using a detection limit of four times the r.m.s. noise in the (global) sky background, determined from the individual images. We did not force our detection routine to constrain the source roundness or sharpness, in order to be as inclusive as possible.

For NGC 3310, at a distance $D \simeq 13$ Mpc (Bottinelli et al. 1984, Kregel & Sancisi 2001), most star clusters and star forming regions appear as point-like sources, and the detection of individual stars among these is unlikely given the associated high luminosities required. Thus, we can use the initial source lists as a starting point to obtain the final, verified list of candidate star clusters, as outlined below.

We cross-correlated the source lists obtained in each pair of subsequent passbands, allowing for only a 1.5-pixel positional mismatch between the individual images. The F606W ⊗ F814W cross-correlated source lists were subsequently adopted as the basis for our final source lists, to which we added the source detections resulting from the cross correlations of the other passband pairs, if not already included.

To reject artefacts remaining in the final source lists and real sources that were badly situated for aperture photometry, we visually examined all of the candidates on enlargements of both of the images from which they originated for contrast, definition, aperture centering, and background sampling. We rejected candidates that were too diffuse or

that might be the effects of background fluctuations. A small number of sources contained multiple components or substructure (as expected for young stellar associations), and the apertures were adjusted to include all of these. We also visually inspected the 2-D Gaussian fits to those sources that were assigned $\sigma_{\rm Gauss} \geq 2$ pixels in the initial automated fitting pass. If needed, apertures for our final photometric pass (and thus the source magnitudes), centre coordinates, and $\sigma_{\rm Gauss}$'s were adjusted. The visual verification is a justifiable step in the reduction process, since – after all – we are mainly interested in obtaining good photometry for a representative, sample of (young) star clusters, for which we can reliably derive the systematic uncertainties in their age, extinction and metallicity determinations. Hence, we sacrifice some sample completeness in order to achieve higher sample reliability.

Thus, our primary cluster candidate samples consist of well-defined sources with $\sigma_{\rm Gauss} \geq 1.20$ pixels and relatively smooth backgrounds. The total number of visually verified sources contained in our source lists is 382 and 289, respectively, for the "*WFPC2*-only" FoV and for the combined FoV.

2.2 Photometric calibration

The coordinates from the source lists obtained in the previous section were used as the centres for DAOPHOT aperture photometry in all passbands.

The correct choice of source and background aperture sizes is critical for the quality of the resulting photometry. Due to the complex structure of the star-forming regions, we concluded that we had to assign apertures for source flux and background level determination individually to each cluster candidate by visual inspection. The "standard" apertures for the majority of the sources were set at a 5-pixel radius for the source aperture and an annulus between 5 and 8 pixels for the background determination, although in individual cases we had to deviate significantly from these values (e.g., because of extended source sizes, contamination by nearby objects, or gradients in the local sky background). Our photometry includes most, if not all, of the light of each cluster candidate.

The photometric calibration, i.e., the conversion of the instrumental aperture magnitudes thus obtained to the *HST*-flight system (STMAG), was done by simply using the appropriate zero-point offsets for each of the individual passbands, after correcting the instrumental magnitudes for geometric distortions, charge transfer (in)efficiency effects, and the exposure times, following procedures identical to those applied in de Grijs et al. (2002).

The full data tables containing the integrated photometry of all clusters are available on-line, at http://www.ast.cam.ac.uk/STELLARPOPS/Starbursts/.

Special care needs to be taken when calibrating the UV aperture magnitudes, in particular the F300W and F336W fluxes. These filters suffer from significant "red leaks" (Biretta et al. 2000, chapter 3). This causes a fraction of an object's flux longward of ~ 6000Å to be detected in these filters. Close inspection of the filter transmission curves reveals that the response curve of the red-leak region of the F300W filter resembles the transmission curve of the F814W filter, being most dominant in the 7000–9000Å

range. The red leak of the F336W filter is roughly similar to the red half of the F814W filter response function. This is fortunate, and implies that we could in principle use our F814W observations to correct the F300W and F336W fluxes for red-leak contamination. Biretta et al. (2000) show that the red leak in these two filters is in general $\lesssim 5\%$ of the total flux for stellar populations dominated by K3V or earlier-type stars, although it can be as much as 10–15% of the total flux for stellar populations dominated by M0V– M8V stars. Thus, for starburst galaxies dominated by young hot stellar populations the red leak contamination should be almost negligible, typically $\lesssim 1\%$.

For realistic spectral energy distributions (SEDs) for early-type galaxies (dominated by older stellar populations), we have shown that the F300W red leak is typically 5–7% of the total F300W flux, and never exceeds the 10% level, not even in the reddest galactic bulges (Windhorst et al. 2002, Eskridge et al. 2003). Adopting Eskridge et al.'s (2003) most straightforward assumption, namely that the red leak cannot account for any more than all of the observed counts in any given area of a few pixels in the F300W and/or F336W images, we derive a maximum contribution of the red leak in NGC 3310 to both the F300W and the F336W filters of 3% of the total count rate *in the F814W image*. We applied these corrections to the F300W and F336W images before obtaining the aperture photometry.

2.3 Completeness analysis

We estimated the completeness of our source lists by using synthetic source fields consisting of PSFs. We created artificial source fields for input magnitudes between 18.0 and 28.0 mag, in steps of 0.5 mag, independently for each of the F300W, F606W, and F814W passbands. We then applied the same source detection routines used for our science images to the fields containing the combined galaxy image and the artificial sources. The results of this exercise, based on the *WFPC2* FoV, are shown in Fig. 1. These completeness curves were corrected for the effects of blending or superposition of multiple randomly placed artificial PSFs as well as for the superposition of artificial PSFs on genuine objects. A detailed description of the procedures employed to obtain these completeness curves was given in de Grijs et al. (2002).

We found that the effects of image crowding are small: only $\lesssim 1.5\%$ of the simulated objects were not retrieved by the DAOFIND routine due to crowding. However, the effects of the bright and irregular background and dust lanes are large, resulting in variable completeness fractions across the central galaxy images. As a general rule, however, the curves in Fig. 1 show that incompleteness becomes severe (i.e. the completeness drops below $\sim 50\%$) for F300W > 22.5 mag, for F606W > 24 mag, and for F814W > 24 mag.

Foreground stars are not a source of confusion (e.g., E02). The standard Milky Way star count models (e.g., Ratnatunga & Bahcall 1985) predict roughly 1–2 foreground stars for the equivalent standard filter of F606W $\lesssim 24$ in the combined *WFPC2* FoV of our images.

Background objects may pose a (small) problem, however, in particular among the fainter sources, since we did not impose any roundness or sharpness constraints on our extended source detections, in order not to omit unrelaxed young clusters from our final sample. However, such objects
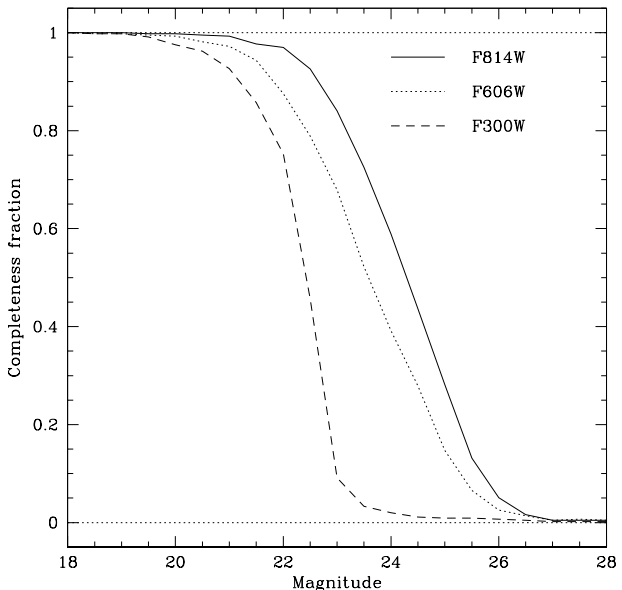

Figure 1. Completeness curves for the *WFPC2* FoV of NGC 3310. The different line styles refer to different passbands, as indicated in the figure.

should be easily identifiable once we have obtained aperture photometry for our complete source lists, as they are expected to have significantly different colours. More quantitatively, background galaxies at redshifts greater than about 0.1 are expected to have extremely red (F300W–F814W) colours compared to their local counterparts.

3 ANALYSIS OF THE STAR CLUSTER PHOTOMETRY

We applied a three-dimensional χ^2 minimisation to the SEDs of our star cluster candidates to obtain the most likely combination of age t, metallicity Z and total (i.e., Galactic foreground and internal) extinction $\mathrm{E}(B - V)$ (assuming a Calzetti et al. [2000] starburst galaxy-type extinction law) for each individual object. Galactic foreground extinction is taken from Schlegel et al. (1998) for each individual object (Section 5; see Anders et al. 2002, 2003). The least-squares minimisation of the clusters' SEDs was done with respect to the Göttingen SSP models (Schulz et al. 2002), to which we added the age and metallicity-dependent contributions of an exhaustive set of gaseous emission lines and gaseous continuum emission (Anders et al. 2002, Anders & Fritze–v. Alvensleben 2003). Their contributions to the broad-band fluxes are most important for significantly subsolar abundances (i.e., $0.2Z_\odot$; because the YSCs *and* the ionised gas are assumed to have the same low metallicity) during the first $\simeq 3 \times 10^7$ yr of their evolution (Anders et al. 2002, Anders & Fritze–v. Alvensleben 2003), while for solar metallicity populations the relative importance is significantly reduced (to roughly half the relative contribution of $0.2Z_\odot$ objects) and of much shorter duration ($t \lesssim 1.2 \times 10^7$ yr).

The Schulz et al. (2002) Göttingen SSP models compose a model grid in age and metallicity covering ranges of $0.02 \leq$

$Z/Z_\odot \leq 2.5$ (as discrete metallicities of $0.02, 0.2, 0.4, 1.0$ and $2.5Z_\odot$) and $1.4 \times 10^8 \leq$ age/yr $\leq 1.6 \times 10^{10}$ yr, in time steps of 1.4×10^8 yr, respectively. They are based on the most recent Padova isochrones and include the thermally pulsing AGB stellar evolutionary phase for stars with masses m in the range $2 \leq m/M_\odot \leq 7$. We also extended the age range of the Göttingen SSP models down to ages as young as 4×10^6 yr in time steps as short as 4×10^6 yr for the youngest ages.

In order to obtain useful fit results for all of our three free parameters, i.e., age, metallicity and extinction[‡], we need a minimum SED coverage of four passbands (or three independent colours). To assess the effects of choosing a particular passband combination on the final results, we started with applying our fitting technique to passband combinations consisting of four filters each, and subsequently added more passbands, as follows:

(i) a blue-selected passband combination, consisting of photometry in the F300W ("UV"), F336W ("U"), F439W ("B") and F606W ("V") filters;

(ii) a subset of only optical passbands: F336W, F439W, F606W and F814W ("I");

(iii) a red-selected passband combination: the red optical F606W and F814W filters, combined with the NIR F110W ("J") and F160W ("H") passbands;

(iv) a five-passband optical/near-infrared combination: F439W, F606W, F814W, F110W and F160W;

(v) the previous combination with the addition of the blue F336W filter; and

(vi) our full set of seven passbands from across the entire wavelength range.

Finally, in Section 5.2 we compare our results from the Göttingen SSP models to independently determined solutions for the same star cluster samples based on the Starburst99 SSP models (Leitherer et al. 1999) for ages below 1 Gyr, and on the Bruzual & Charlot (2000; BC00) models for older ages. The fitting of the observed cluster SEDs to the Starburst99 and BC00 models was done using a three-dimensional maximum likelihood method, "3/2DEF", with the initial mass M_i, age and extinction E$(B - V)$ as free parameters (see Bik et al. 2003), and assuming a fixed, solar metallicity, a Salpeter-type initial mass function (IMF), and the (Galactic) extinction law of Scuderi et al. (1996). We will discuss the uncertainties introduced by the assumption of solar metallicity below. For the clusters with upper limits in one or more filters we used a two-dimensional maximum likelihood fit, using the extinction probability distribution for E$(B - V)$. This distribution was derived for the clusters with well-defined SEDs over the full wavelength range (see Bik et al. 2003).

[‡] Strictly speaking, the cluster mass is also a free parameter. Our model SEDs are valid for SSPs with masses of $1.6 \times 10^9 M_\odot$; to obtain the actual cluster mass, we scale the model SED to match the observed cluster SED using a single scale factor. This scale factor is then converted into a cluster mass.

4   SETTING THE SCENE: THE YOUNG MERGER REMNANT NGC 3310

NGC 3310 is a local, very active starburst galaxy with high global star formation rate, as is evident from its bright optical and infrared continuum emission (Telesco & Gatley 1984 [hereafter TG84], Braine et al. 1993, Mulder, van Driel & Braine 1995 [hereafter MvDB95], Díaz et al. 2000 [hereafter D00], E02), strong and extended X-ray, UV, and thermal radio emission (van der Kruit & de Bruyn 1976, Code & Welch 1982, Fabbiano, Feigelson & Zamorani 1982, Zezas, Georgantopoulos & Ward 1998, Conselice et al. 2000), intense UV and optical emission lines typical of OB associations (Heckman & Balick 1980, Kinney et al. 1993, Mulder et al. 1995 and references therein) and its large global Hα equivalent width (MvDB95, Mulder & van Driel 1996 [hereafter MvD96], and references therein).

4.1   A peculiar starburst galaxy

A number of morphological peculiarities in its outer parts (e.g., Balick & Heckman 1981, Kregel & Sancisi 2001, [hereafter BH81, KS01], MvD96), combined with the disturbed kinematics of the H$_I$ gas in the inner regions (e.g., van der Kruit 1976, MvDB95, KS01), the mismatch between stellar and gas-dynamical geometry (e.g., BH81), and the large number of early-type stars required to explain the galaxy's Hα emission (van der Kruit 1976, BH81), suggest that NGC 3310 was affected by a major gravitational disturbance. This led to high, possibly sustained, star formation rates in the past ~ 100 Myr (cf. BH81). Since attempts to identify a nearby companion galaxy as the cause for the disruption and the expected subsequent major starburst were unsuccessful (cf. van der Kruit 1976, van der Kruit & de Bruyn 1976), it was suggested that NGC 3310 accreted a gas-rich, but metal-poor companion galaxy, which subsequently fragmented as a result of the encounter (BH81, Schweizer & Seitzer 1988, MvDB95, MvD96, Smith et al. 1996, hereafter S96; modeled by Athanassoula 1992 and Piner, Stone & Teuben 1995), or perhaps we are currently seeing a newly-formed disc. This argument was based predominantly on the absence of any close companion galaxy and on the unusually low (subsolar) metallicity found in star forming regions surrounding the nucleus, although the nucleus itself appears to have solar metallicity (e.g., Heckman & Balick 1980, Puxley, Hawarden & Mountain 1990, Pastoriza et al. 1993, hereafter P93). Additional support for this interpretation is provided by the far-ultraviolet and B-band $R^{1/4}$ luminosity profiles, typical of late-stage galaxy mergers (S96, KS01), and the optical and H$_I$ tails and ripples observed in the outer parts.

The galaxy's most conspicuous visual peculiarity is the well-studied bright optical "bow and arrow" structure (nomenclature first used by Walker & Chincarini 1967). The "arrow" is a jet-like structure with possibly an H$_I$ counterpart (although the latter is significantly more extended; MvDB95), which has been interpreted as the result of a nuclear explosive event some 1.8×10^7 yr ago (Bertola & Sharp 1984), or – in combination with the ripple pattern that includes the "bow" – as the result of a recent merger with a smaller companion galaxy (or even a third, smaller object; KS01). The latter explanation seems more likely (see MvDB95, KS01). These authors argued that a "projectile"

object hitting the disc of NGC 3310 at a fairly oblique angle could have been drawn out into the observed configuration, which is supported by the anomalous velocity structure observed within these features (MvDB95); the optical "arrow" is then best understood as a series of regions in which active star formation was triggered due to the collision. If this scenario is correct, the merger event must have occurred $\lesssim 10$ Myr ago to prevent significant redistribution of the longer H I jet due to differential rotation (cf. MvDB95), although the outer jet regions appear to curve away from the line of sight (KS01, see also MvDB95).

4.2 Star cluster formation

The bar-driven star formation scenario suggested by Conselice et al. (2000), combined with the recent infall of a companion galaxy, is very attractive: it provides a natural explanation for the low metallicity observed in the star-forming knots near the centre, while it also explains why we observe concentrated star formation in star clusters or very luminous H II regions in a tightly-wound ring-like structure surrounding the centre (e.g., van der Kruit & de Bruyn 1976, TG84, P93, Meurer et al. 1995, S96, Conselice et al. 2000, E02), coinciding with the end of the nuclear bar (Conselice et al. 2000, but see D00), but not inside this ring.

The most luminous single star-forming region in NGC 3310 is the giant "Jumbo" H II region (BH81, TG84, S96); it is roughly $10\times$ more luminous than 30 Doradus in Hα (BH81), but it is of very low metallicity, $Z \sim 0.1 Z_\odot$ (P93). The Jumbo H II region contains several individual UV-bright star clusters (Meurer et al. 1995, E02). The most luminous star-forming structure is the ring of H II regions, which produces some 30% of the observed far-UV flux of NGC 3310 (S96). We have indicated our cluster detections in Fig. 2, overlaid on our press release image of the galaxy (Windhorst et al. 2001).

Numerous other, less luminous star clusters and H II regions, with sizes from 10 pc for the most luminous ones to $\lesssim 1$ pc for the unresolved clusters in the background disc (see Conselice et al. 2000), are found scattered in the galaxy's outer parts beyond $R \simeq 4$ kpc (van der Kruit & de Bruyn 1976, BH81, TG84, MvDB95, S96) and as condensations in the "bow and arrow" structure (e.g., Bertola & Sharp 1984, S96, KS01); these clusters may have been produced by the accretion event, or might be remnants of the progenitor companion galaxy (cf. BH81, S96).

4.3 Star formation time-scales

All of the observational evidence points at very recent star formation in the star clusters and H II regions, and a time since the interaction of $\lesssim 10^7 - 10^8$ yr (van der Kruit 1976, BH81, TG84, P93, S96, E02): the optical colours and the equivalent widths of the Hα-bright circumnuclear sources are best reproduced by a combination of a 2.5 Myr and an 8 Myr-old population (cf. P93, D00). This is consistent with *(i)* the detection of WR features in the spectra of a few of the H II regions, including the Jumbo region, and of the NIR Ca II triplet (Terlevich et al. 1990, P93), both indicative of stellar populations with ages $\lesssim 4$ Myr, and *(ii)* the absence of significant non-thermal radio emission (cf. TG84),

which implies that there is not yet a significant population of supernova remnants. Terlevich et al. (1990) found evidence for two stellar populations (of 5 and 15 Myr old) as well, which can also be interpreted as an extended star formation episode. As pointed out by TG84 (see also MvDB95), the star formation in NGC 3310 can continue at its present rate only for a small fraction of the age of the galaxy, roughly $4 \times 10^7 - 10^8$ yr, depending on the IMF assumed (MvDB95).

5 AGE DETERMINATIONS: SYSTEMATIC UNCERTAINTIES

5.1 Dependence on the SED coverage

We obtained 156, 145, 100, 85, 63 and 60 solutions from our least-squares minimisation technique (for our age, metallicity and extinction determinations), respectively, for the six passband combinations chosen for the analysis of the NGC 3310 photometry (see Sect. 3) in the small FoV covered by the full passband combination. The relatively small fraction of acceptable solutions mainly reflects the rather low S/N ratios in a number of our archival images, resulting in either large photometric uncertainties or upper limits for the aperture photometry. Since the main aim of this paper is to analyse the dependence on the choice of passband combination of the resulting ages, extinction values and metallicities, objects containing upper limits to their photometry in any of the passbands in a given passband combination were excluded from the fitting procedure. We emphasize once again that we used exactly the same sample of star clusters, with well-determined photometric measurements in *all* passbands (as defined above), for this comparison. Acceptable solutions were required to have fit values for *each* photometric measurement in a given passband combination within the 2σ observational uncertainty associated with that particular filter; weights were allocated proportional to $1/\chi^2$.

Fig. 3 shows the dependence of the resulting age distribution on the choice of passband combination. The shaded histograms represent the acceptable age solutions (with minimum χ^2 values obtained from the least-squares minimisation) for the cluster sample in common among all six passband combinations; the open histograms are the additional solutions obtained for the respective passband combinations. The uncertainties in the *number* of clusters in a given age bin are predominantly Poissonian; the uncertainties in the actual ages are the subject of our current analysis. The electronic data tables containing our best solutions for all passband combinations are also available from the aforementioned WWW address. It is immediately clear from this figure that the resulting age distribution of an extragalactic star cluster system based on broad-band colours is a sensitive function of the passbands covered by the observations.

To guide the eye, we have overplotted – on all panels – the best-fit Gaussian age distribution based on the full, 7-passband SED sampling (Fig. 3f). This best-fit age distribution is characterized by a peak at $\log(\text{age/yr}) = 7.51 \pm 0.12$ and a Gaussian width of $\sigma_{\text{Gauss}} = 0.33$, irrespective of the bin size adopted.

From a comparison of the age distributions in Fig. 3, we determine that:

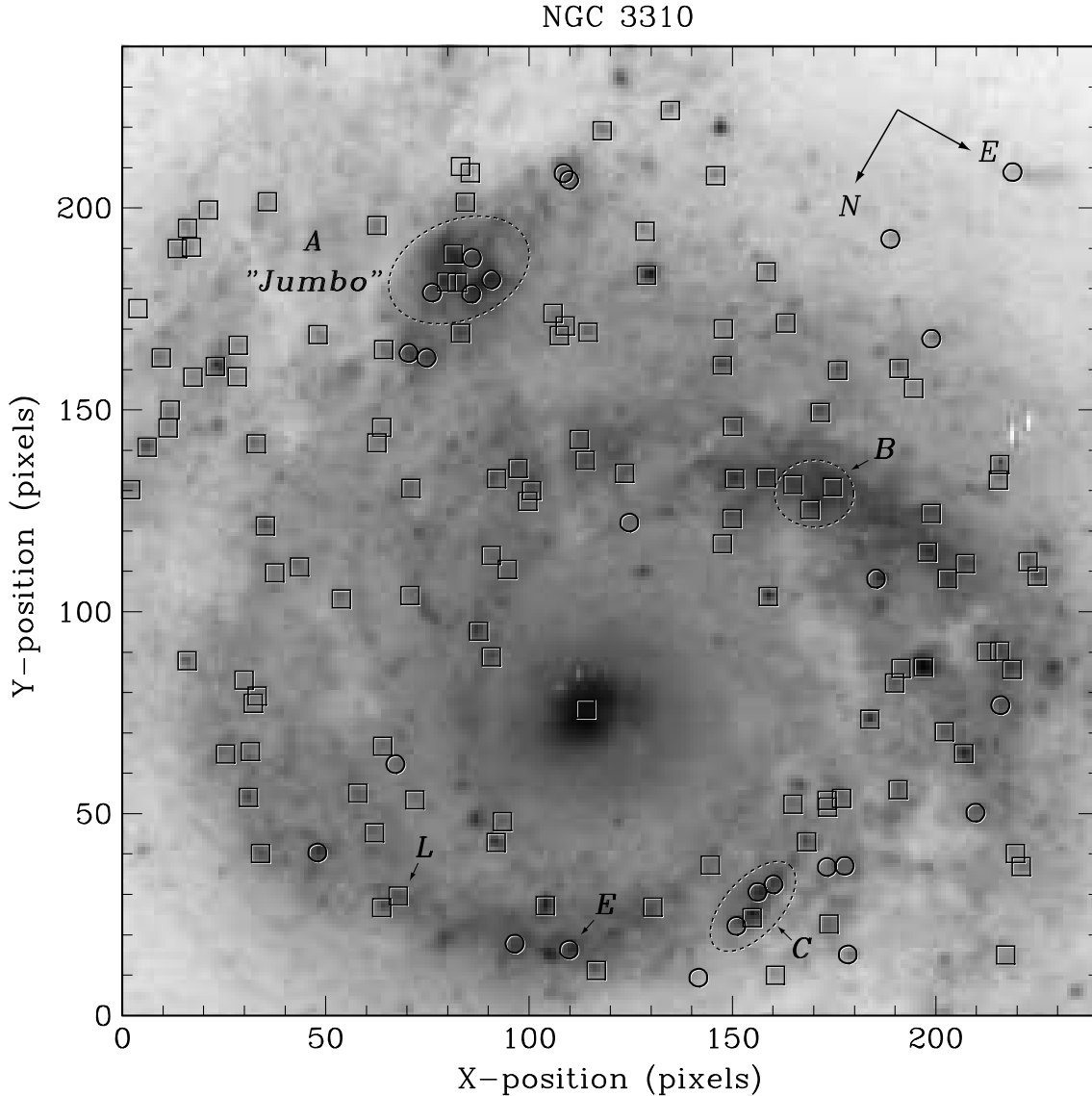• the peak of the age distribution is robustly reproduced

NGC 3310

Figure 2. Cluster detections in NGC 3310, for which we obtained acceptable solutions for all of their ages, metallicities, and extinction values (see Sect. 5.1) overlaid on a grey-scale rendition of our F300W press release image of the galaxy (Windhorst et al. 2001, 2002). The circles represent sources younger than $\log(\text{age/yr}) = 7.1$, the squares are the older objects. The nomenclature of sources A–C, E, and L is from P93.

in all cases, for both the shaded and the full cluster samples with acceptable solutions, except for the red-selected passband combination (Fig. 3c);

• photometric measurements in red-dominated passband combinations (Figs. 3c and d) result in significantly older (but highly uncertain) age solutions. This is due to the weak time dependence of the NIR magnitudes and due to unavoidable ambiguities in the modelling of the thermally pulsing AGB phase, thus resulting in badly constrained "best" fit ages. Red-dominated age solutions produce a significant wing of older clusters, compared to the ages derived from the full passband combination.

• blue-selected passband combinations (such as in Figs. 3a and b; open histograms) tend to result in age estimates that are slightly skewed towards younger ages, compared to passband combinations that also include redder passbands. This is simply due to the combination of observational selec-

tion effects, in the sense that younger clusters have higher UV and *U*-band fluxes and are therefore more easily detected at those blue wavelenghts, and to the age–metallicity degeneracy (see below). Such secondary peaks at young ages should therefore be treated with extreme caution.

• the optical passband combination (Fig. 3b), in particular, displays a distinct secondary peak at very young ages, $\log(\text{age/yr}) \sim 6.7$ (cf. open histogram). These clusters do not appear to be exceptional in their metallicity, extinction or mass properties compared to the overall distribution of these properties among the other clusters in our sample. However, with few exceptions, we could not obtain satisfactory solutions for these clusters as part of our full passband combination fits. As we will show below, this secondary peak is most likely the result of the age–metallicity degeneracy.

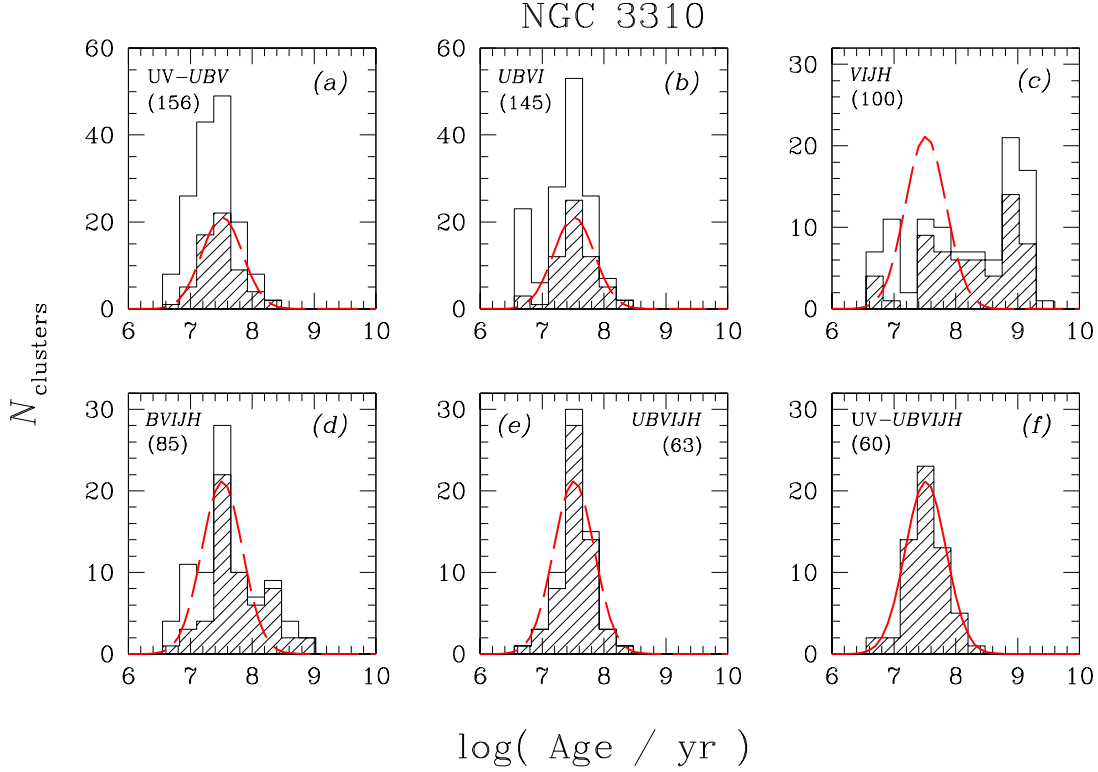In Fig. 4 we illustrate the sensitivity of the parameter

NGC 3310

Figure 3. Relative age distributions of the NGC 3310 clusters based on six choices of broad-band passband combinations, with acceptable solutions. The shaded histograms represent the cluster sample with acceptable solutions in common among all six passband combinations (60 clusters); the open histograms are the additional solutions obtained for subsamples based on the passband combination displayed in each panel. The numbers in between brackets in each panel correspond to the total number of clusters in the histograms. We have overplotted the best-fit Gaussian age distribution obtained in panel f.

determinations on the available passband combination by showing the SEDs and best fits for three typical, representative clusters, located in P93 regions "C" (Fig. 4a; cluster No. 18) and "B" (Figs. 4b and c; Nos. 116 and 122, respectively). The dotted lines represent the best-fitting models based on a blue-selected passband combination, the dash-dotted lines were derived from the red-selected combination, while the dashed and solid fits are based on the full passband combination and on the subset of $UBVI$ filters only, respectively. In Table 2 we list the best-fitting free parameters as a function of passband combination used for all three clusters, to illustrate the effects of our choice of wavelength coverage.

Note that all of our conclusions apply to the YSC population in NGC 3310, characterised by ages in the range from $\sim 10^6$ to $\sim 10^9$ yr. The situation may be significantly different for clusters of significantly greater age. Thus, from an observational point of view, for ages $6 \lesssim \log(\text{age/yr}) \lesssim 9$, we conclude that if one can only obtain partial coverage of a star cluster's SED, an optical passband combination including *both* blue *and* red optical passbands results in the best balanced and most representative age distribution, as compared to the better constrained ages obtained from the full UV–NIR SED coverage. While blue-selected passband combinations lead to age distributions that are slightly biased towards younger ages, red-selected passband combinations – in particular if they are dominated by NIR filters – should clearly be avoided.

Table 2. Dependence of our fit parameters on the available passband combination for three representative clusters

Passbands	log(Age) [yr]	log(Mass) [$M_\odot$]	Metallicity (Z)	E($B - V$) (mag)
	Cluster No. 18 (from Region "C")			
UV−UBV	7.205	5.666	0.022	0.05
$UBVI$	6.876	5.356	0.008	0.00
$VIJH$	6.660	5.304	0.013	0.25
UV−$UBVIJH$	7.204	5.512	0.002	0.00
	Cluster No. 116 (from Region "B")			
UV−UBV	7.362	5.968	0.011	0.08
$UBVI$	7.448	5.939	0.008	0.06
$VIJH$	8.939	6.770	0.002	0.06
UV−$UBVIJH$	7.478	5.911	0.012	0.06
	Cluster No. 122 (from Region "B")			
UV−UBV	6.986	5.474	0.012	0.13
$UBVI$	7.276	5.577	0.010	0.10
$VIJH$	8.071	6.079	0.003	0.12
UV−$UBVIJH$	7.349	5.636	0.012	0.11

5.2 The age–metallicity degeneracy

Finally, in Fig. 5 we compare the best-fit age distributions of the clusters in the small FoV covered by all seven passbands, and the larger "*WFPC2*-only" FoV, covered by our five optical passbands. These best-fit age distributions were derived from either the full, seven/five passband SED cov-
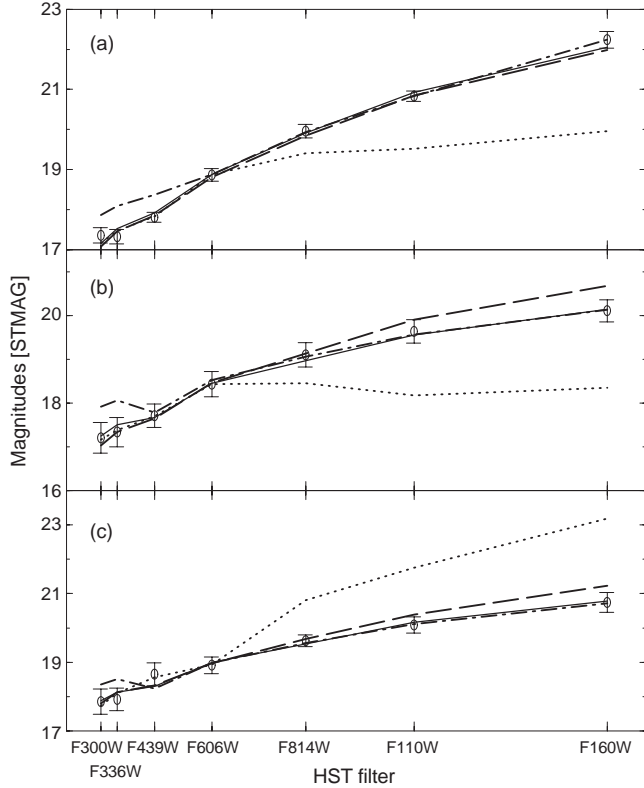
Figure 4. Illustration of the sensitivity of the parameter determinations on the available passband combination for three representative clusters in regions "C" (panel a) and "B" (panels b and c). The dotted lines represent the best-fitting models based on a blue-selected passband combination, the dash-dotted lines were derived from the red-selected combination, while the dashed and solid fits are based on the full passband combination and on the subset of $UBVI$ filters only, respectively. The *HST* filters are spaced according to their central wavelengths.

erage if acceptable solutions could be obtained for all of our free parameters, or from the passband combination with the highest "confidence ranking", in a minimum χ^2 sense: we defined a confidence ranking among the passband combinations, such that a higher ranking was given to solutions obtained from a passband combination (i) containing more passbands, (ii) covering a larger wavelength base line and (iii) resulting in a smaller χ^2 value.

For comparison, in Fig. 5a we have – once more – overplotted the best-fit Gaussian age distribution obtained from the full SED sampling of the same (small) FoV, as in Fig. 3f. The vertical error bars represent the Poissonian uncertainties dominating the cluster numbers in each age bin. In Fig. 5b we show both the age distribution of the clusters in the large FoV (solid histogram) and again the age distribution in the small FoV, overplotted as the dashed histogram (both normalised by the total number of clusters in each sample), in order to illustrate the apparent $\sim (2-2.5)\sigma$ peak at young ages, $\log(\text{age/yr}) \lesssim 6.8$.

A naive interpretation of this feature would suggest that the outer field of NGC 3310, outside the small FoV, contains a subpopulation of significantly younger clusters. However, closer inspection of our data reveals that this young peak is entirely owing to unavoidable systematic uncertainties in-

herent to our fitting technique and the shape of the SED. It turns out that the secondary, young peak is caused by the limited number of passbands available for the full cluster sample in the *WFPC2*-only FoV, due to the lack of NIR photometry for the clusters outside the small FoV. If we restrict our fits of the age, extinction and metallicity properties of the cluster sample in the *small* FoV to the same *WFPC2*-only passbands, we find a similar young age peak in the inner FoV, of similar strength and significance.

The clusters contained in this latter young-age peak are characterized by a smoother age distribution (ranging from $\sim 5 \times 10^6$ to $\sim 2 \times 10^7$ yr, with a few outliers as old as $\sim 10^8$ yr) in the best-fit age distribution based on the full UV–NIR SED sampling. In addition, while these clusters are all characterized by a narrow spread in metallicity around $\sim 0.5 Z_\odot$ in the restricted fit using the *WFPC2* passbands only, their metallicity estimates range from $\sim 0.02 Z_\odot$ to $\sim 2.5 Z_\odot$ if we take the full UV–NIR SED into account. Thus, we conclude that the secondary age peak at young ages in the *WFPC2*-only FoV is an artefact caused by the age–metallicity degeneracy at ages younger than about 10^8 yr. The age–extinction degeneracy is not as significant as this age–metallicity degeneracy, for these particular clusters. The slight, $\sim 2\sigma$ excess of young clusters in the youngest age bin of Fig. 5a may be a remaining systematic effect, or may indeed be marginal evidence of more recent cluster formation.

To illustrate this point, in the top panel of Fig. 6 we show the age dependence of the model SEDs for solar metallicity. Next, in the bottom panel we explore the effects of varying the metallicity for the youngest, 8 Myr-old SED. For illustrative purposes we also show the effects of adding $E(B-V) = 0.5$ mag extinction to the solar-metallicity SED (dashed line with solid bullets). The grey vertical lines are drawn at the central wavelengths of the F606W (or F555W) and F814W *HST* filters often used for age dating of individual clusters. It is clear that for these young ages, the effects of varying the metallicity, extinction or age of the stellar population cannot be disentangled unless one has access to observations in a larger number of passbands, which may allow to more robustly constrain all of the free fitting parameters.

Finally, in Fig. 7 we compare our best fit age distribution (dashed Gaussian distribution) with the best fit age distribution using the Bik et al. (2003) approach. The latter is based on the Starburst99/BC00 SSP models, and a fixed metallicity of $Z = Z_\odot$. While the differences between the age distributions resulting from fitting the Göttingen or the Starburst99/BC00 models are expected to be random due to the use of different stellar evolutionary tracks and different template spectra for (super)giant stars (see Schulz et al. 2002), the assumption of fixed, solar metallicity causes the fitting technique to produce a significantly different age distribution compared to the distribution obtained by leaving the metallicity as a free parameter. We confirmed this result by fitting the individual cluster ages and extinction values using the Göttingen SSP models, while keeping the metallicity fixed at solar values. This is, again, a clear signature of the age–metallicity degeneracy. We point out that this is, in fact, an expected effect, since unusually low (subsolar) metallicities were found in NGC 3310's star forming regions (e.g., Heckman & Balick 1980, Puxley, Hawarden &
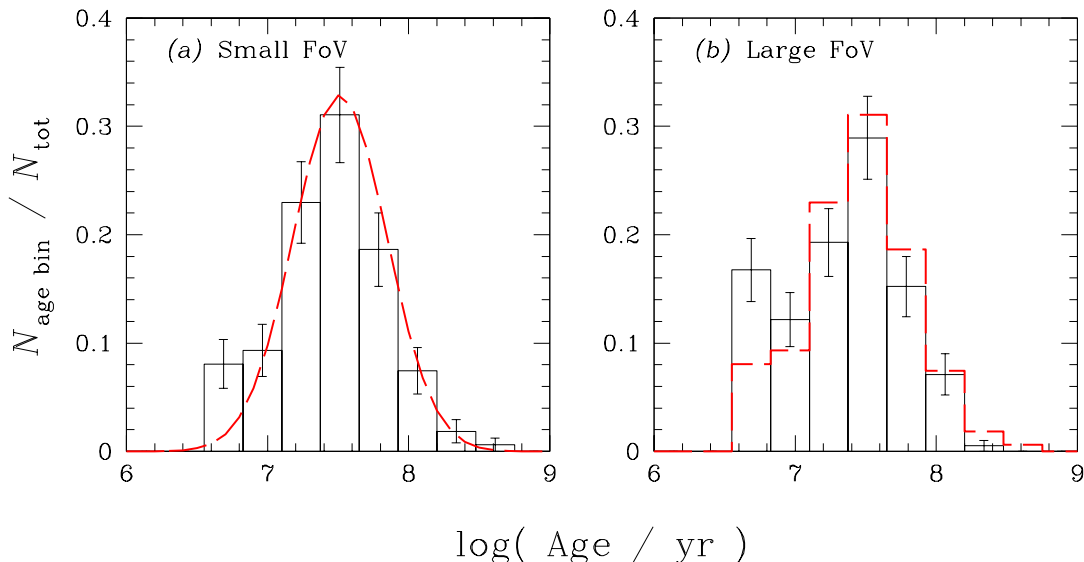
Figure 5. Comparison of the age distributions of the NGC 3310 star clusters in the small, inner FoV and the large, *WFPC2*-only FoV. The error bars represent Poissonian uncertainties in the numbers of clusters in each age bin. The dashed Gaussian distribution (panel a) is our best-fit age distribution (Fig. 3f); the dashed histogram overplotted on the large FoV age distribution (panel b) is the age distribution of the small FoV.

Mountain 1990, P93, D00; $Z \sim (0.2 - 0.4)Z_\odot$), so that the assumption of solar metallicity for these sources must have a significant systematic effect.

5.3 Metallicity and extinction estimates

Figure 8 shows our best estimates of the global distribution of metallicity, and of total extinction (i.e., Galactic foreground and internal extinction) towards the NGC 3310 clusters. At first sight, the metallicity and extinction distributions obtained from either of the passband combinations used for Fig. 8 appear very similar within the (systematic) uncertainties. The effects of the age–metallicity degeneracy for the optical passbands (Fig. 8a) are clearly visible. Based on the *UBVI* passband combination only, we find that the metallicity distribution of the clusters in NGC 3310 is strongly dominated by significantly subsolar metallicities, while the addition of NIR passbands results in the detection of a significant number of clusters with metallicities $Z \sim 2.5Z_\odot$. In either case, the fact that the resulting metallicity determinations are strongly dominated by (significantly) subsolar metallicities is encouraging, in view of independent metallicity measurements in the literature. Both the low and higher-metallicity objects are distributed fairly smoothly across the face of the galaxy; there is some evidence that the most actively star forming regions, in particular the Jumbo region and the northern spiral arm (including complex C), are predominantly composed of lower-abundance star clusters.

Similarly, the addition of NIR passbands appears to result in more solutions with lower extinction estimates (Figs. 8e and f). This is likely due to the better constraints on the extinction from optical-NIR compared to optical-only baselines. However, whether this result is indeed significant also depends on the suitability of the starburst galaxy-type extinction law adopted for our fitting routine (Calzetti et al. 2000), of which the analysis is beyond the scope of the present paper (but see Calzetti, Kinney, & Storchi-Bergmann [1994] for a discussion). Nevertheless, these effects are negligible, or marginally significant at worst, compared to the photometric uncertainties ($\sim 0.10 - 0.15$ mag).

6 NGC 3310 IN ITS PHYSICAL CONTEXT

6.1 Overall properties of the NGC 3310 cluster population

We can conclude from this exercise that NGC 3310 underwent a significant burst of cluster formation some 3×10^7 yr ago. The actual duration of the burst of cluster formation may have been shorter because uncertainties in the age determinations may have broadened the peak. It appears, therefore, that the peak of cluster formation in NGC 3310 coincides closely with the suspected galactic cannibalism or last tidal interaction (van der Kruit 1976, BH81, TG84, P93, S96, E02), while the possibly more recent, marginally significant cluster formation at $t \lesssim 10^7$ yr can be interpreted as cluster formation associated with the most recent ($\lesssim 10$ Myr) enhanced star formation episode traced by the circumnuclear Hα-bright sources (P93, D00).

The clusters older than $\sim 10^7$ yr are smoothly distributed throughout the galactic centre, roughly following the inner ring structure and the other concentrations of star clusters (see Fig. 2). However, the younger clusters, with ages $\log(\text{age/yr}) \le 7.1$ (i.e., the youngest two age bins in Fig. 3), are predominantly concentrated in the Jumbo region ("A"; nomenclature from P93) and in the northern spiral arm, which also contains the bright star-forming regions C and E (see Fig. 2). This is consistent with the very young ages derived for these regions, $t \lesssim 10$ Myr (Terlevich et
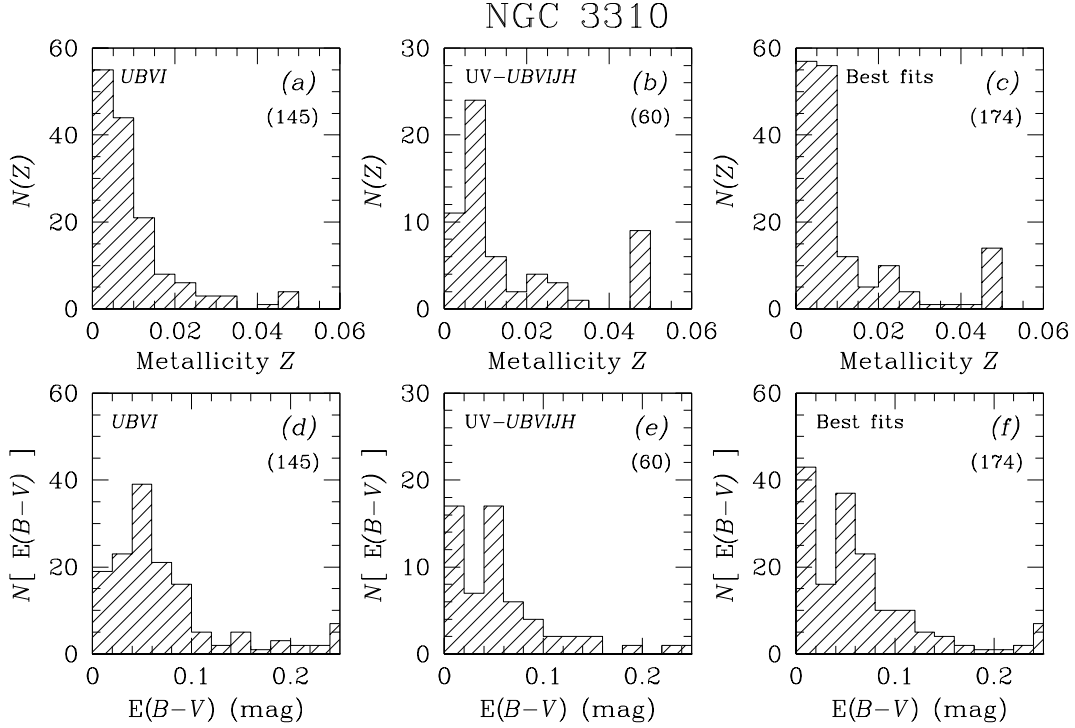
Figure 8. Distributions of metallicity, and of total extinction towards the NGC 3310 clusters for the solutions from a number of passband combinations. The numbers in between parentheses correspond to the total number of clusters represented by each histogram.

al. 1990, P93, D00, E02), although we emphasize that both regions also contain clusters spanning the entire age range observed for the NGC 3310 star cluster system.

Figure 9 shows our best estimates of the clusters' masses. These were obtained by scaling our model SEDs (for masses of $1.6 \times 10^9 M_\odot$) to the observed SEDs for the appropriate combination of age, metallicity and (total) extinction. Our model SEDs are based on a Salpeter-type IMF consisting of stellar masses m in the range $0.15 \leq m/M_\odot \leq (50 - 70)$ (Schulz et al. 2002). The exact upper mass limit for our model SSPs depends on the metallicity and is determined by the mass coverage of the Padova isochrones. The exact value for the upper mass limit is unimportant for the determination of the total cluster masses.

We realise that recent determinations of the stellar IMF deviate significantly from a Salpeter-type IMF at low masses, in the sense that the low-mass stellar IMF may well be significantly flatter than the Salpeter slope. The implication of using a Salpeter-type IMF for our cluster mass determinations is therefore that we may have *overestimated* the individual cluster masses (although the relative mass distribution of our entire cluster sample remains unaffected). Therefore, we used the more modern IMF parametrisation of Kroupa, Tout & Gilmore (1993, hereafter KTG) to determine the correction factor, C, between our masses and the masses obtained from the KTG IMF (both normalised at $1.0 M_\odot$). This IMF is characterised by slopes of $\alpha = -2.7$ for $m > 1.0 M_\odot$, $\alpha = -2.2$ for $0.5 \leq m/M_\odot \leq 1.0$, and $-1.85 < \alpha < -0.70$ for $0.08 < m/M_\odot \leq 0.5$. Depending on the adopted slope for the lowest mass range, we have therefore overestimated our individual cluster masses by a factor

of $1.5 < C < 2.4$ for an IMF containing stellar masses in the range $0.15 \leq m/M_\odot \lesssim 70$.

The mass distributions derived from the different passband combinations are fairly similar. We determined the defining parameters of the cluster mass distributions by fitting Gaussian distributions to them. The small differences among the median mass [$\langle \log(m/M_\odot) \rangle = 5.22, 5.29$, and 5.21 for Figs. 9a, b and c, respectively] and Gaussian widths of the distributions (similarly varying among $\sigma_{\text{Gauss}} = 0.32, 0.34$, and 0.34, respectively) represent the minimum systematic uncertainties in these parameter determinations (minimum because they are based on our highest-confidence passband combinations). In view of the uncertainties introduced by the badly known lower-mass slope of the adopted IMF, the median mass estimates of the NGC 3310 cluster system are remarkably close to those of the Galactic GC system and of the intermediate-age cluster system in M82 B (de Grijs et al. 2003a,b).

6.2 Comparison of individual cluster results with previous determinations

Although both NGC 3310 as such and its star cluster system in particular have been studied extensively, determinations of individual cluster ages, masses, metallicities and extinction values are rare. The most extensive cluster sample useful for a comparison to the results presented in this paper was published by E02. They estimate masses and ages of (a subset of) 11 large-scale, diffuse cluster complexes (see also D00) and of 17 super star cluster (SSC) candidates based on *HST* photometry; the latter were also noted by Conselice
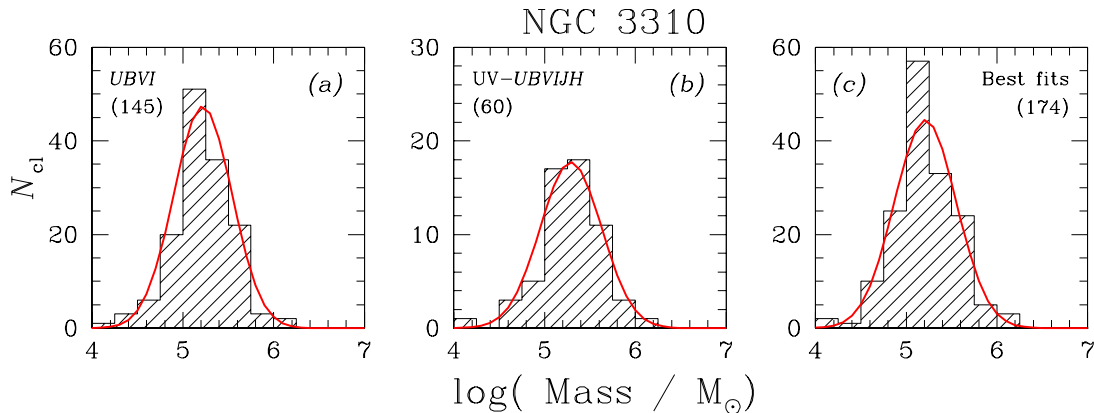
Figure 9. Mass distributions for the NGC 3310 clusters for a number of passband combinations. Overplotted are the best-fit Gaussian distributions (solid lines). The numbers in between brackets correspond to the total number of clusters represented by each histogram.

et al. (2000). In Table 3 we compare the E02 mass and age determinations for their sample of SSC candidates, based on the assumption of a mean metallicity of $Z = 0.008 = 0.4Z_\odot$, with the corresponding parameters derived in this paper.

We give our mass estimates for two assumptions of the lower mass limit of the Salpeter-type IMF; varying the upper mass limit has very little effect. While we have used a lower mass limit of $0.15M_\odot$ throughout this paper (resulting in the mass estimates $M_{\rm tot,1}$), E02's cluster mass estimates ($M_{\rm tot,cf}$) are based on the Starburst99 models, which assume a lower mass cut-off of $1M_\odot$. Everything else being equal, our resulting mass estimates are therefore expected to be a factor of ~ 13 higher compared to theirs. Our total mass estimates assuming a lower mass cut-off of $1M_\odot$ are referred to as $M_{\rm tot,2}$.

A first comparison of our individually derived metallicity estimates shows that E02's assumption of a mean cluster metallicity of $0.4Z_\odot$ (based on spectroscopic metallicity determinations by P93) is reasonable, except for a few clusters with significantly supersolar abundances. Secondly, our low extinction values are also in line with our expectations for the circumnuclear ring clusters; although the extinction in the starburst ring varies in the range $1 \lesssim A_V \lesssim 4$ mag (Grotheus & Schmidt-Kaler 1991), is has been shown that circumnuclear ring clusters are often either almost fully obscured or virtually dust free (e.g., Maoz et al. 2001). In addition, Meurer et al. (1995) estimate the average extinction in the NGC 3310 starburst regions to be in the range $0.18 \lesssim {\rm E}(B - V) \lesssim 0.23$, based on the slope of the UV SED and published Balmer decrement measurements (P93), respectively, and P93 estimated $0.13 \lesssim {\rm E}(B - V) \lesssim 0.37$ based on spectroscopic measurements (see also S96, D00). Since these extinction estimates cover both the YSCs and the ISM, they are consistent with being upper limits to the extinction towards individual YSCs.

For their large-scale complexes, E02 assumed a mean age of $\sim 10^7$ yr, which is somewhat underestimated compared to our mean age of the individual clusters in these complexes of $\sim 4 \times 10^7$ yr. For the "Jumbo" region (E02 complex 108+109), P93 derived an age of 1.45×10^7 yr from spectrophotometry, which is consistent with the median age

we derive for the clusters in this region, $t_{\rm Jumbo} \sim 1.3 \times 10^7$ yr.
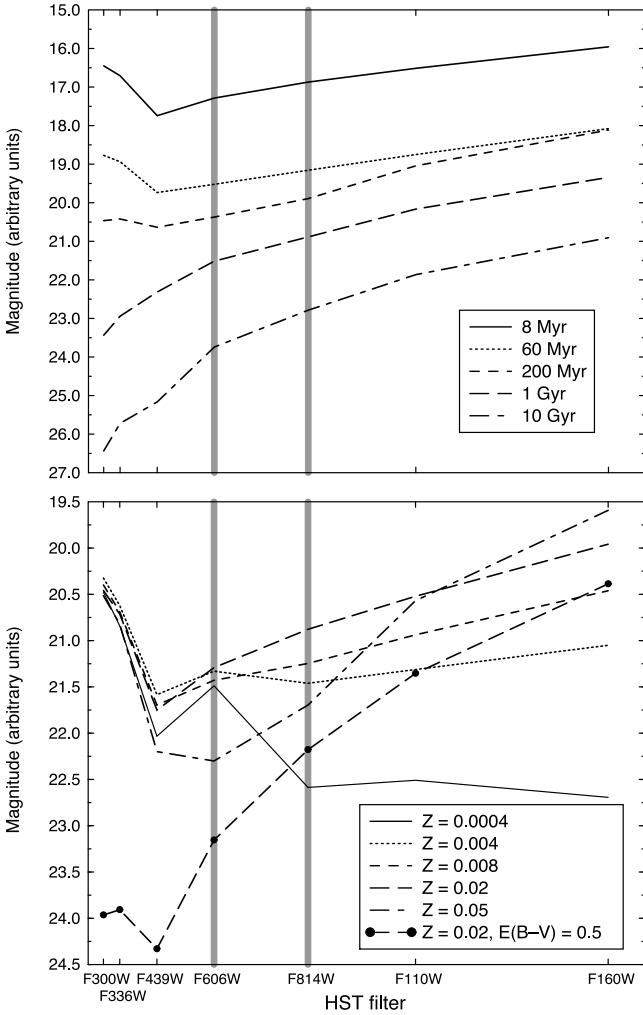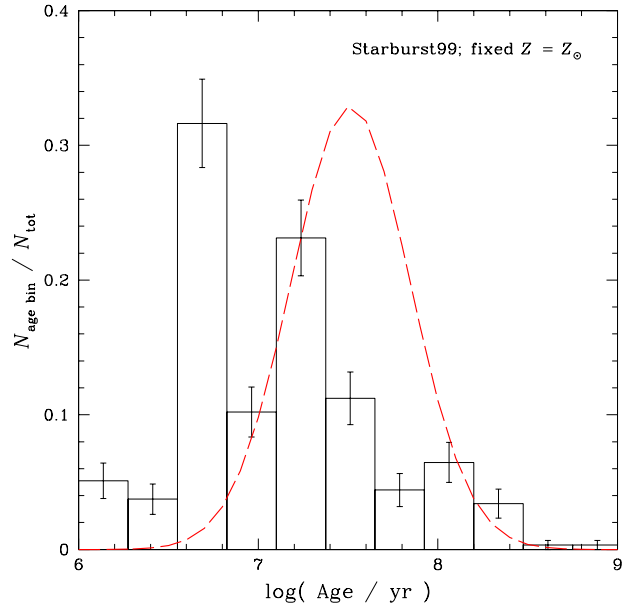
Although the match between our individual cluster age estimates and the E02 results is good for clusters 8 (E02 estimate $\sim 20 - 30$ Myr; our estimate ~ 26 Myr), 19 ($\sim 20 - 30$ vs. ~ 21 Myr) and 64 ($10 - 50$ vs. 33 Myr), and reasonable for clusters 36 ($\lesssim 5 - 10$ vs. $\sim 9 - 10$ Myr) and 90 ($10 - 50$ vs. 14 Myr), it is poor for clusters 37 ($\sim 1 - 5$ vs. ~ 16 Myr; this is no surprise, because our models do not extend to such young ages), 49 ($10 - 50$ vs. 94 Myr), and 59 ($10 - 50$ vs. 320 Myr). Owing to the strong age-dependence of the M/L ratio at those young ages, small differences in our age estimates *will* have significant consequences for the final mass determinations, for ages in the range determined for the NGC 3310 clusters. In addition, the difference in the assumed distance modulus to NGC 3310 between ourselves ($D = 13$ Mpc; Sect. 2.1) and E02 ($D = 18.7$ Mpc) of ~ -0.8 mag introduces an additional uncertainty to the clusters' luminosity of $\Delta \log L \simeq 0.3$, corresponding to a factor of ~ 2 in luminosity, and therefore in the mass (via the M/L ratio) as well, in the sense that we expect the E02 mass estimates to be $\sim 2\times$ higher.

Thus, from a comparison between our final masses and those of E02, we conclude that the factor of $2 - 3$ between most of our mass estimates, in the sense that E02's masses are the higher, is not too surprising in view of the many uncertainties involved in (i) the difference in distance to NGC 3310 assumed, (ii) the different methods used for our mass estimates, (iii) the different ways in which we obtained our aperture photometry and the subsequent photometric calibrations (E02 converted their measurements to the standard ground-based system, while we continued in the STMAG system), and (iv) the different models employed (cf. Fritze–v. Alvensleben 2000). Regarding the latter, we point out that these differences may have been augmented by our inclusion of nebular emission (which we have shown to be important for ages younger than $\sim 3 \times 10^7$ yr; Anders et al. 2002, Anders & Fritze–v. Alvensleben 2003) and our approach to solve for all of our free parameters simultaneously.

This comparison clearly shows that while we can obtain robust relative distributions of masses, ages, and metallicities for a given star cluster system fairly easily (as shown

Table 3. Comparison of our derived cluster parameters with those of the E02 SSC candidates.

Number (E02)	log(Age) [yr]	log(Mass) $[M_\odot]$	Metallicity (Z)	$E(B-V)$ (mag)	$M_{\rm tot,1}$ $(10^5 M_\odot)$	$M_{\rm tot,2}$ $(10^4 M_\odot)$	$M_{\rm tot,cf}$ $(10^4 M_\odot)$
8	7.412	5.529	0.009	0.05	3.4	2.6	9
19	7.331	6.175	0.001	0.00	15.0	11.5	45
32	8.182	5.722	0.050	0.00	5.3	4.1	8
36	6.989	5.629	0.001	0.09	4.3	3.3	6
37	7.204	5.512	0.001	0.00	3.3	2.5	7
49	7.973	6.006	0.008	0.15	10.1	7.8	8
59	8.505	5.935	0.012	0.12	8.6	6.6	2
64	7.512	5.077	0.050	0.00	1.2	0.9	2
80	7.369	5.133	0.028	0.00	1.4	1.0	2
81	7.136	4.832	0.008	0.05	0.7	0.5	2
85	7.982	6.021	0.008	0.05	10.5	8.1	8
90	7.139	4.935	0.050	0.00	0.9	0.7	3
107	8.035	5.521	0.012	0.03	3.3	2.6	5

Figure 6. *(top panel)* Age dependence of the model SEDs for solar metallicity. *(bottom panel)* Metallicity dependence of the 8 Myr-old model SED. we also show the effects of adding $E(B-V) = 0.5$ mag extinction to the solar-metallicity SED (dashed line with solid bullets). The *HST* filters are spaced according to their central wavelengths. The grey vertical lines are drawn at the central wavelengths of the F606W (or F555W) and F814W *HST* filters often used for age dating of individual clusters.

Figure 7. Age distribution of the NGC 3310 star clusters based on a comparison of their SEDs with the Starburst99 models and fixed, solar metallicity. The dashed Gaussian distribution is our best-fit age distribution from a comparison with the Göttingen SSP models, leaving the metallicity as a free parameter. The error bars represent Poissonian uncertainties in the numbers of clusters in each age bin.

throughout this paper), the absolute calibration, and therefore the absolute mass, age and metallicity scales can only be fixed robustly if we have access to independent *spectroscopic* measurements of these parameters.

6.3   The NGC 3310 Cluster Luminosity Function

The importance of correcting the observed CLFs to a common age cannot be overemphasized. Age spread effects in young cluster systems, and therefore the combined effects of ongoing cluster formation, evolutionary fading, and the onset of cluster disruption, affect the observed CLF (cf. Meurer 1995, Fritze–v. Alvensleben 1999, de Grijs et al. 2001, 2003a,b). This implies that the CLF observed in such

a system represents merely a temporal situation, rather than a characteristic property of a coeval cluster system.

Using the age estimates obtained for the individual clusters, we corrected the F606W magnitudes of our cluster sample to a common age of $10^{7.5}$ yr using the Anders & Fritze-v. Alvensleben (2003) models properly folded through the *HST/WFPC2* F606W filter response curve, for the "best-fit" age distribution of Fig. 5a. In order to provide a comparison with the CLFs of other young cluster systems, we employed the Levenberg-Marquardt method (Marquardt 1963) to fit power-law slopes of the form $N(L) \propto L^{\alpha}$ (where L is the luminosity of a cluster, and α the power-law slope) to both CLFs.

In the V-band luminosity range $10^6 \leq L_{\mathrm{F606W}}/L_{\odot} \leq 10^7$ ($17.7 \lesssim \mathrm{F606W} \lesssim 20.2$ mag), the slope of the CLF is $\alpha = -1.4 \pm 0.2$, and $\alpha = -1.8 \pm 0.4$ for the full, uncorrected sample of clusters, and for the "best-fit" sample corrected to a common age of $\log(\mathrm{age/yr}) = 7.5$, respectively.

In de Grijs et al. (2001) and Parmentier et al. (2002) we showed that the constant-age V-band CLF for the bright clusters in M82's post-starburst region "B" roughly follows a power law with a slope in the range $-1.4 \lesssim \alpha \lesssim -1.2$, which is consistent with the power-law slopes of other young CLFs, and within the uncertainties also with the NGC 3310 CLF. On the other hand, D00 found a significantly shallower slope of $\alpha \sim -1$ for the Hα-bright circumnuclear star forming regions in NGC 3310 (but we note that these are likely the youngest objects populating the CLF, with ages $\lesssim 6-12$ Myr, depending on metallicity), while E02 obtained slopes as steep as $(-2.4 \pm 0.04) \leq \alpha \leq (-2.2 \pm 0.03)$ from their B and K-band cluster measurements, which is – within the uncertainties – consistent with our V-band determination. The main uncertainties that are expected to affect the CLF slope in this latter case are the luminosity range over which the slopes were obtained, and the fact that E02 did not correct their CLFs to a common age before measuring their slopes.

7 SUMMARY AND CONCLUSIONS

7.1 Systematic uncertainties

In this paper we have investigated the systematic uncertainties involved in using broad-band UV, optical and NIR observations to derive age, mass, metallicity and extinction distributions for extragalactic star cluster systems. The large majority of extragalactic star cluster studies done to date have essentially used two or three-passband aperture photometry, combined with theoretical stellar population synthesis models to obtain age estimates. The accuracy to which this can be done obviously depends on the number of different (broad-band) filters available as well as, crucially, on the actual wavelengths and the wavelength range covered by the observations. Understanding these systematic uncertainties is therefore of the utmost importance for a well-balanced interpretation of the properties of such star cluster systems.

We focused our analysis on the nearby, well-studied starburst galaxy NGC 3310, known to harbour large numbers of young star clusters, for which we obtained multipassband observations from the UV to the NIR from the *HST* Data Archive. We used our evolutionary synthesis op-

timisation technique to simultaneously determine the best combination of age, extinction and metallicity.

Our main results can be summarised as follows. For a star cluster system as young as that in NGC 3310,

• the peak of the age distribution is robustly reproduced for all of our choices of passband combinations, except for the red-only selected filter combination;

• red-dominated passband combinations result in significantly different (uncertain) age solutions, due to the weak time dependence of the NIR magnitudes and due to unavoidable ambiguities in the modelling of the thermally pulsing AGB phase; they produce a significant wing of older clusters.

• blue-selected passband combinations tend to result in age estimates that are slightly skewed towards younger ages, compared to passband combinations that also include redder passbands. This is due to the combination of observational selection effects and to the age–metallicity degeneracy, which is also of importance in passband combinations containing only optical filters.

• for ages $6 \lesssim \log(\mathrm{age/yr}) \lesssim 9$, we conclude that if one can only obtain partial coverage of a star cluster's SED, an optical passband combination of at least 4 filters including *both* blue *and* red optical passbands results in the best balanced and most representative age distribution. While blue-selected passband combinations lead to age distributions that are slightly biased towards younger ages, red and in particular NIR-dominated passband combinations should be avoided.

• The physical effect most limiting the accuracy of our age determinations, for ages up to $\sim 10^8$ yr, is the age–metallicity degeneracy. This is clearly illustrated in our comparison with results obtained assuming a fixed, solar metallicity. If the actual cluster metallicities are significantly subsolar, this assumption results in a markedly different age distribution, biased towards younger ages, compared to the distribution obtained by leaving the metallicity as a free parameter.

7.2 The NGC 3310 cluster system

NGC 3310 is a local, very active starburst galaxy with high global star formation efficiency, which has experienced very recent star formation in star clusters and H II regions, in the last $\lesssim 10^7 - 10^8$ yr. In the inner FoV covered by all of our passbands, we detected some 300 star cluster candidates, while an additional ~ 100 clusters were detected in the outer FoV covered by the *WFPC2* filters only, all of them affected by only moderate levels of NGC 3310-internal extinction towards the clusters, $\mathrm{E}(B-V) \lesssim 0.1$ mag. The age distribution derived for these clusters indicates that NGC 3310 underwent a significant burst of cluster formation some 3×10^7 yr ago. The actual duration of the burst of cluster formation, which we estimate to have lasted for almost 20 Myr, may have been shorter because uncertainties in the age determinations may have broadened the peak. It appears, therefore, that the peak of cluster formation in NGC 3310 coincides closely with the suspected galactic cannibalism or last tidal interaction.

The clusters older than $\sim 10^7$ yr are smoothly distributed throughout the galactic centre. However, the younger clusters, with ages $\log(\mathrm{age/yr}) \leq 7.1$, are predomi-

nantly concentrated in the Jumbo region and in the northern spiral arm. This is consistent with the very young ages independently derived for these regions, $t \lesssim 10$ Myr, although both regions also contain clusters spanning the entire age range observed for the NGC 3310 star cluster system.

The CLF is the result of a complex interplay of the intrinsic cluster mass distribution, age spread and cluster disruption processes. We therefore determined the individual cluster masses by scaling our model SEDs for the best-fit age, extinction values and metallicity estimates to the observed SEDs. We estimate the cluster system to have a median mass of $\langle \log(m/M_\odot) \rangle \sim 5.25 \pm 0.1$, not including systematic uncertainties introduced by the uncertainties in the low-mass IMF slope.

Our metallicity determinations are strongly dominated by (significantly) subsolar metallicities, which is consistent with independent metallicity measurements. There is some evidence that the most actively star forming regions, in particular the Jumbo region and the northern spiral arm, are predominantly composed of lower-abundance star clusters. The V-band CLF slope in the range $10^6 \leq L_{\mathrm{F606W}}/L_\odot \leq 10^7$ for the NGC 3310 star cluster system is $\alpha_{\mathrm{F606W}} \sim -1.8 \pm 0.4$, which is consistent with the power-law slopes of other young CLFs.

Finally, we point out that our estimates for the ages, masses, metallicities and extinction values of the YSCs in NGC 3310 closely match previous, independent determinations of these parameters, where available (e.g., Grotheus & Schmidt-Kaler 1991, P93, Meurer et al. 1995, D00, E02). This implies, to first order, that this type of analysis is reasonably robust.

ACKNOWLEDGMENTS

REFERENCES

Anders P., Fritze-v. Alvensleben U., 2003, A&A, in press (astro-ph/0302146)

Anders P., Fritze-v. Alvensleben U., de Grijs R., 2002, in: The Evolution of Galaxies. III – From Simple Approaches to Self-Consistent Models, eds. Hensler G., et al., Kluwer: Dordrecht, in press (astro-ph/0210223)

Anders P., Fritze-v. Alvensleben U., de Grijs R., 2003, MNRAS, in prep.

Athanassoula E., 1992, MNRAS, 259, 345

Balick B., Heckman T., 1981, A&A, 96, 271 (BH81)

Bertola F., Sharp N.A., 1984, MNRAS, 207, 47

Bik A., Lamers H.J.G.L.M., Bastian N., Panagia N., Romaniello M., 2003, A&A, 397, 473

Biretta J.A., et al., 2000, *WFPC2* Instrument Handbook, Version 5.0 (Baltimore: STScI)

Bottinelli L., Gougenheim L., Paturel G., de Vaucouleurs G., 1984, A&AS, 56, 381

Boutloukos S.G., Lamers H.J.G.L.M., 2003, MNRAS, 338, 717

Braine J., Combes F., Casoli F., Dupraz C., Gerin M., Klein U., Wielebinski R., Brouillet N., 1993, A&AS, 97, 887

Bruzual G., Charlot S., 2000, updated version of Bruzual G., Charlot S., 1996, in: Leitherer, C., et al. 1996, PASP, 108, 996 (AAS CDROM Series 7) (BC00)

Calzetti D., Armus L., Bohlin R.C., Kinney A.L., Koornneef J., Storchi-Bergmann T., 2000, ApJ, 533, 682

Calzetti D., Kinney A.L., Storchi-Bergmann T., 1994, ApJ, 429, 582

Carlson M.N., et al., 1998, AJ, 115, 1778

Code A., Welch G., 1982, ApJ, 256, 1

Conselice C.J., Gallagher J.S., Calzetti D., Homeier N., Kinney A.L., 2000, AJ, 119, 79

de Grijs R., Bastian N., Lamers H.J.G.L.M., 2003a, MNRAS, in press (astro-ph/0211420)

de Grijs R., Bastian N., Lamers H.J.G.L.M., 2003b, ApJ, 583, L17

de Grijs R., Johnson R.A., Gilmore G.F., Frayn C.M., 2002, MNRAS, 331, 228

de Grijs R., O'Connell R.W., Gallagher J.S., 2001, AJ, 121, 768

Díaz A.I., Álvarez Álvarez M., Terlevich E., Terlevich R., Sánchez Portal M., Aretxaga I., 2000, MNRAS, 311, 120 (D00)

Elmegreen B.G., Efremov Y.N., 1997, ApJ, 480, 235

Elmegreen D.M., Chromey F.R., McGrath E.J., Ostenson J.M., 2002, AJ, 123, 1381 (E02)

Elson R.A.W., Fall S.M., 1985, PASP, 97, 692

Eskridge P.B., et al., 2003, ApJ, in press (astro-ph/0211494)

Fabbiano G., Feigelson E., Zamorani G., 1982, ApJ, 256, 397

Fall S.M., Rees M.J., 1977, MNRAS, 181, 37P

Fall S.M., Rees M.J., 1985, ApJ, 298, 18

Fall S.M., Zhang Q., 2001, ApJ, 561, 751

Ferguson A.M.N., Gallagher J.S., Wyse R.F.G., 1998, AJ, 116, 673

Fritze-v. Alvensleben U., 1998, A&A, 336, 83

Fritze-v. Alvensleben U., 1999, A&A, 342, L25

Fritze-v. Alvensleben U., 2000, in Lançon A., Boily C., eds., ASP Conf. Ser. Vol. 211, Massive Stellar Clusters, Astron. Soc. Pac., San Francisco, p. 3

Fritze-v. Alvensleben U., Gerhard O.E., 1994, A&A, 285, 751

Gnedin O.Y., Ostriker J.P., 1997, ApJ, 474, 223

Grotheus H.G., Schmidt-Kaler T., 1991, A&A, 242, 357

Harris W.E., 1996, AJ, 112, 1487

Harris W.E., 2001, in: Star Clusters, Saas-Fee Advanced Course 28, Springer-Verlag, 223

Harris W.E., Harris G.L.H., McLaughlin D.E., 1998, AJ, 115, 1801

Harris W.E., Pudritz R.E., 1994, ApJ, 429, 177

Heckman T.M., Balick B., 1980, A&AS, 40, 295

Hibbard J.E., Mihos J.C., 1995, AJ, 110, 140

Kinney A.L., Bohlin R.C., Calzetti D., Panagia N., Wyse R.F.G., 1993, ApJS, 86, 5

Kobulnicky H.A., Skillman E.D., 1995, ApJ, 454, L121

Kregel M., Sancisi R., 2001, A&A, 376, 59 (KS01)

Kroupa P., Tout C.A., Gilmore G.F., 1993, MNRAS, 262, 545

Leitherer C., Schaerer D., Goldader J.D., Gonzalez Delgado R.M., Robert C., Kune D.F., de Mello D.F., Devost D., Heckman T.M., 1999, ApJS, 123, 3 (Starburst99)

Maoz D., Barth A.J., Ho L.C., Sternberg A., Filippenko A.V., 2001, AJ, 121, 3048

Maoz D., Barth A.J., Sternberg A., Filippenko A.V., Ho L.C., Macchetto F.D., Rix H.-W., Schneider D.P., 1996, AJ, 111, 2248

Marquardt D.W., 1963, J. of the Soc. for Industrial and Applied Mathematics, 11, 431

Martin C.L., Kennicutt R.C., Jr., 1995, ApJ, 447, 171

McLaughlin D.E., Pudritz R.E., 1996, ApJ, 457, 578

Mengel S., Lehnert M.D., Thatte N., Tacconi-Garman L.E., Genzel R., 2001, ApJ, 550, 280

Meurer G.R., 1995, Nat, 375, 742

Meurer G.R., Heckman T.M., Leitherer C., Kinney A., Robert C., Garnett D.R., 1995, AJ, 110, 2665

Miller B.W., Whitmore B.C., Schweizer F., Fall S.M., 1997, AJ, 114, 2381

Mirabel I.F., et al., 1998, A&A, 333, L1

Murali C., Weinberg M.D., 1997a, MNRAS, 288, 749

Murali C., Weinberg M.D., 1997b, MNRAS, 288, 767

Murali C., Weinberg M.D., 1997c, MNRAS, 291, 717

Mulder P.S., van Driel W., 1996, A&A, 309, 403 (MvD96)

Mulder P.S., van Driel W., Braine J., 1995, A&A, 300, 687 (MvDB95)

Oey M.S., Kennicutt R.C., Jr., 1993, ApJ, 411, 137

Ostriker J.P., Gnedin O.Y., 1997, ApJ, 487, 667

Parmentier G., de Grijs R., Gilmore G., 2002, MNRAS, submitted

Pastoriza M.G., Dottori H.A., Terlevich E., Terlevich R., Díaz A.I., 1993, MNRAS, 260, 177 (P93)

Piner B.G., Stone J.M., Teuben P.J., 1995, ApJ, 449, 508

Puxley P.J., Hawarden T.G., Mountain C.M., 1990, ApJ, 364, 77

Richer M.G., McCall M.L., 1995, ApJ, 445, 642

Ratnatunga K.U., Bahcall J.N., 1985, ApJS, 59, 63

Schlegel D.J., Finkbeiner D.P., Davis M., 1998, ApJ, 500, 525

Schulz J., Fritze–v. Alvensleben U., Möller C.S., Fricke K.J., 2002, A&A, 392, 1

Schweizer F., Miller B.W., Whitmore B.C., Fall, S.M., 1996, AJ, 112, 1839

Schweizer F., Seitzer P., 1988, ApJ, 328, 88

Scuderi S., Panagia N., Gilmozzi R., Challis P.M., Kirshner R.P., 1996, ApJ, 465, 956

Smith D.A., et al., 1996, ApJ, 473, L21 (S96)

Stetson P.B., 1987, PASP, 99, 91

Telesco C.M., Gatley I., 1984, ApJ, 284, 557 (TG84)

Terlevich E., Díaz A.I., Pastoriza M.G., Terlevich R., Dottori H., 1990, MNRAS, 242, 48P

van der Kruit P.C., 1976, A&A, 49, 161

van der Kruit P.C., de Bruyn A.G., 1976, A&A, 48, 373

van Zee L., Salzer J.J., Haynes M.P., O'Donoghue A.A., Balonek T.J., 1998, AJ, 116, 2805

Vesperini E., 2000, MNRAS, 318, 841

Vesperini E., 2001, MNRAS, 322, 247

Walker M.F., Chincarini G., 1967, ApJ, 147, 416

Whitmore B.C., Schweizer F., 1995, AJ, 109, 960

Whitmore B.C., Schweizer F., Leitherer C., Borne K., Robert C., 1993, AJ, 106, 1354

Whitmore B.C., Schweizer F., Kundu A., Miller B.W., 2002, AJ, 124, 147

Whitmore B.C., Sparks W.B., Lucas R.A., Macchetto F.D., Biretta J.A., 1995, ApJ, 454, L73

Windhorst R.A., et al., 2001, NASA press release, STScI-PR01-04, 11 January 2001 (http://hubblesite.org/newscenter/archive/2001/04/)

Windhorst R.A., et al., 2002, ApJS, 143, 113

Zaritsky D., Kennicutt R.C., Jr., Huchra J.P., 1994, ApJ, 420, 87

Zepf S.E., Ashman K.M., English J., Freeman K.C., Sharples R.M., 1999, AJ, 118, 752

Zezas A.L., Georgantopoulos I, Ward M.J., 1998, MNRAS, 301, 915